nature photonics

LETTERS

PUBLISHED ONLINE: 5 DECEMBER 2016 | DOI: 10.1038/NPHOTON.2016.240

Solution-processed organic tandem solar cells with power conversion efficiencies >12%

Miaomiao Li[1,2†], Ke Gao[3†], Xiangjian Wan[1,2*], Qian Zhang[1,2], Bin Kan[1,2], Ruoxi Xia[3], Feng Liu[4], Xuan Yang[1,2], Huanran Feng[1,2], Wang Ni[1,2], Yunchuang Wang[1,2], Jiajun Peng[5], Hongtao Zhang[1,2], Ziqi Liang[5], Hin-Lap Yip[3], Xiaobin Peng[3*], Yong Cao[3] and Yongsheng Chen[1,2*]

An effective way to improve the power conversion efficiency of organic solar cells is to use a tandem architecture consisting of two subcells, so that a broader part of the solar spectrum can be used and the thermalization loss of photon energy can be minimized[1]. For a tandem cell to work well, it is important for the subcells to have complementary absorption characteristics and generate high and balanced (matched) currents. This requires a rather challenging effort to design and select suitable active materials for use in the subcells. Here, we report a high-performance solution-processed, tandem solar cell based on the small molecules DR3TSBDT and DPPEZnP-TBO, which offer efficient, complementary absorption when used as electron donor materials in the front and rear subcells, respectively. Optimized devices achieve a power conversion efficiency of 12.50% (verified 12.70%), which represents a new level of capability for solution-processed, organic solar cells.

Organic solar cells (OSCs) have received an extensive amount of attention for renewable energy sources because of advantageous features such as low cost, flexibility, light weight and solution-based fabrication[2]. Recently, as a result of extensive studies and a deeper understanding of OSC mechanisms, new active-layer material design and device optimization, OSC performance has improved dramatically. Power conversion efficiencies (PCEs) have now reached 10–11% for single-junction cells[3–6]. In general, due to the limited absorption range of the active materials in single-junction cells, a large proportion of solar irradiation cannot be used. A useful approach to overcome this problem is to construct a tandem device by stacking, in series, multiple photoactive layers with complementary absorption spectra[7–9], as is done in many current commercial solar cells. For a typical tandem cell consisting of two single cells connected via an interconnection layer, the photon-to-electron conversion process can be described briefly as follows: (1) absorption of photons and free carrier generation; (2) collection of electrons from the front subcell and holes from the rear subcell by the interconnection layer (and vice versa in an inverted device); (3) recombination of the collected electron and holes in the interconnection layer; (4) charge collection of holes in the front subcell and electrons in the rear subcell by the external circuit (and vice versa in an inverted device). One of the characteristics of an ideal set-up is that the open-circuit voltage V_{oc} of the serial connected tandem cell equals the sum of the V_{oc} values of the subcells and no potential loss occurs in the interconnection layer. Furthermore, optimized subcells, with matched but the highest possible current in all subcells, are required in order to achieve a high short-circuit current density J_{sc} in the tandem cells. In addition, it is critical to have an efficient and well-designed interconnection layer with good hole and electron recombination ability.

During the past decade, various interconnection layers have been proposed and successfully used in tandem devices[10,11]. However, all-solution-processed interconnection layers are more attractive so as to be compatible with the printing process used for OSCs. Solution-processed interconnection layers such as poly(3,4-ethylenedioxythiophene)-poly(styrenesulfonate) (PEDOT:PSS)/ZnO nanoparticles[12] and conjugated polyelectrolyte/ZnO[13] have been successfully used in tandem cells. In addition, many wide- and low-bandgap materials, especially polymers, have been used as donor materials in the front and rear subcells of tandem devices[7,8,12,14–17]. However, many of them suffer from the disadvantages of either serious overlap of the absorption spectra or low photovoltaic efficiency in the single cells, which limits the final tandem device performance. For the front subcells, poly(3-hexylthiophene-2,5-diyl) (P3HT) is predominantly used as a donor with acceptor [6,6]-phenyl-C61-butyric acid methyl ester ($PC_{61}BM$)[14] and has also been combined with the acceptor indene-C_{60}-bisadduct (ICBA) in order to improve V_{oc} (refs 7,12). However, its relatively low J_{sc} (around 10 mA cm^{-2}) is a bottleneck for tandem cells constructed with P3HT:ICBA as the front subcell. Other reported wide-bandgap polymers, such as poly[2,7-(9,9-didecylfluorene)-alt-5,5-(4′,7′-di-2-thienyl-2′,1′,3′-benzothiadiazole)] (PFTBT)[15], poly[*N*-9′-heptadecanyl-2,7-carbazole-alt-5,5-(4′,7′-di-2-thienyl-2′,1′,3′-benzothiadiazole)] (PCDTBT)[16], polyindaceno-dithiophene-alt-quinoxaline (PIDT-PhanQ)[11] and poly[5,5′-bis(2-butyloctyl)-(2,2′-bithiophene)-4,4′-dicarboxylate-alt-5,5′-2,2′-bithiophene] (PDCBT)[8], also suffer from similar problems. Much more attention has been targeted at the design of low-bandgap polymers with absorption in the near-infrared range for the rear subcell. Some low-bandgap polymers such as poly[2,7-(5,5-bis-(3,7-dimethyloctyl)-5H-dithieno[3,2-b:2′,3′-d]pyran)-alt-4,7-(5,6-difluoro-2,1,3-benzothiadiazole)] (PDTP-DFBT)[7], poly[(4,8-bis(5-(octylthio)thiophen-2-yl)benzo[1,2-b:4,5-b′] dithiophene-co-3-fluorothieno[3,4-b]thiophene-2-carboxylate] (PBDT-TS1)[8] and several diketopyrrolopyrrole (DPP)-based polymers[16,17] show redshifted absorption over ~850 nm and have been used in the rear subcell of tandem devices. However, the unbalanced J_{sc}, low V_{oc} and low fill factor (FF) of these low-bandgap polymer-based subcells have significantly limited the overall performance

[1]The Centre of Nanoscale Science and Technology and Key Laboratory of Functional Polymer Materials, State Key Laboratory and Institute of Elemento-Organic Chemistry, Collaborative Innovation Center of Chemical Science and Engineering (Tianjin), College of Chemistry, Nankai University, Tianjin 300071, China. [2]School of Materials Science and Engineering, The National Institute for Advanced Materials, Nankai University, Tianjin 300071, China. [3]Institute of Polymer Optoelectronic Materials and Devices, State Key Laboratory of Luminescent Materials and Devices, South China University of Technology, Guangzhou 510640, China. [4]Materials Science Division, Lawrence Berkeley National Lab, Berkeley, California 94720, USA. [5]Department of Material Science, Fudan University, Shanghai 200433, China. †These authors contributed equally to this work.
*e-mail: yschen99@nankai.edu.cn; xjwan@nankai.edu.cn; chxbpeng@scut.edu.cn

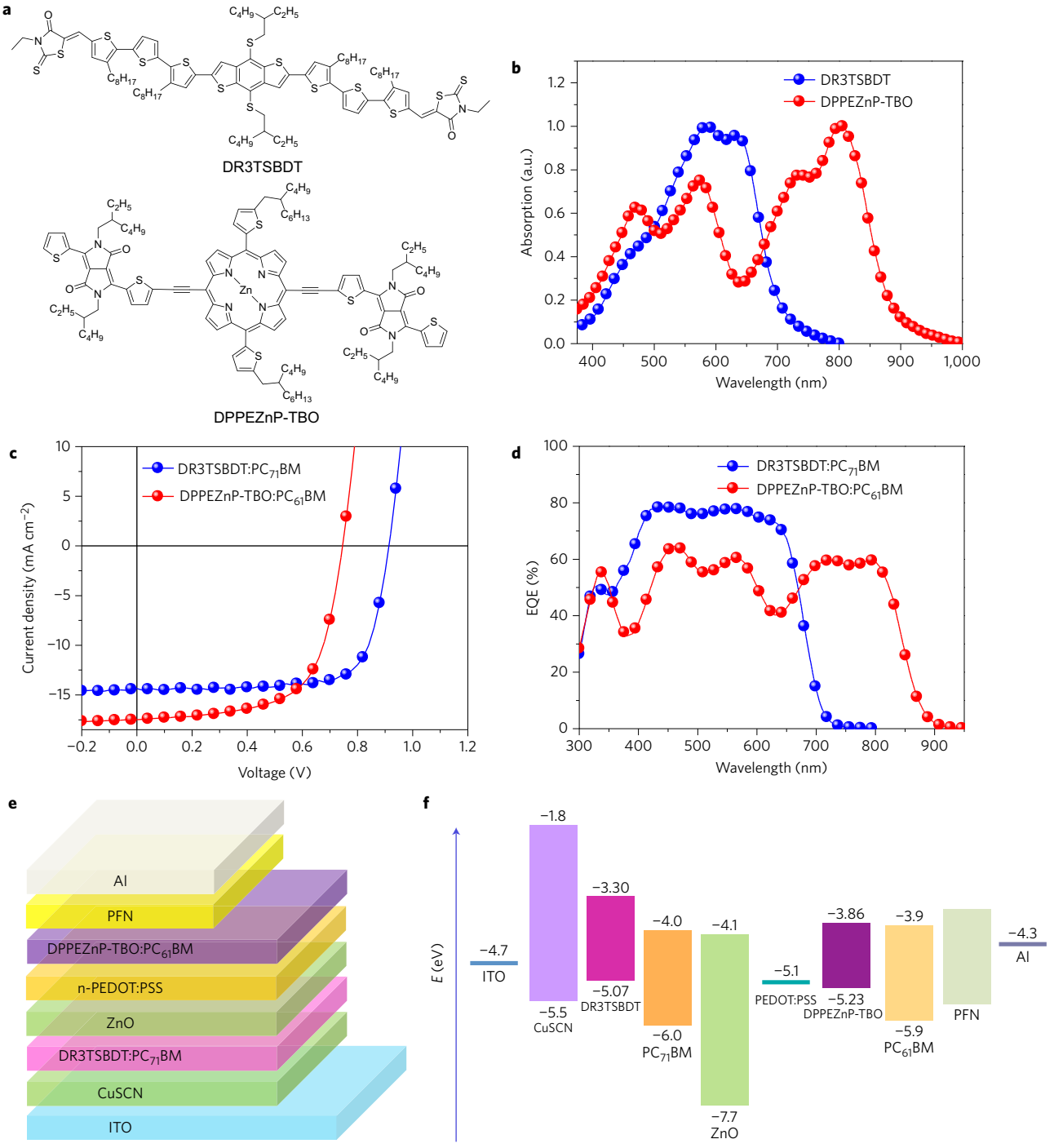

Figure 1 | Molecular structures, photovoltaic performance of the single-junction devices and tandem device architecture. a, Molecular structures of DR3TSBDT and DPPEZnP-TBO. **b**, Normalized absorption spectra of DR3TSBDT and DPPEZnP-TBO films. **c**,**d**, *J*–*V* curves (**c**) and EQE curves (**d**) of the single-junction devices based on DR3TSBDT and DPPEZnP-TBO with an architecture of ITO/PEDOT:PSS/active layer/PFN/Al. **e**, Device architecture of the tandem solar cell. **f**, Energy diagram of the tandem solar cell.

of the created tandem devices. So far, the PCEs of polymer-based tandem cells have been below 12% as a consequence of the above issues, with a best value of 11.62% (ref. 18) for double-junction cells and 11.83% (ref. 9) for three-junction cells.

In recent years, small-molecule donor materials have drawn an increasing amount of attention, for example because of their versatile but defined chemical structures and thus easier energy level control, mobility tuning and reduced batch-to-batch variation[19,20]. It is notable that small-molecule-based devices generally have a relatively high V_{oc} (refs 19,21), which is favourable to tandem cells. Surprisingly, however, studies on tandem devices based on small molecules, especially solution-processed small molecules, lag far behind those focusing on polymer-based tandem devices. So far there have only been a few reports on small-molecule-based tandem cells (a PCE of 10.1% has been achieved[22]) and most were fabricated using an evaporation process (http://www.heliatek.com/en/press/press-releases/details/heliatek-sets-new-organic-photovoltaic-world-record-efficiency-of-13-2)[22,23]. Just recently, we have reported tandem cells that make use of three small molecules ((5Z,5′E)-5,5′-((5′′,5′′′′′-(4,8-bis((2-ethylhexyl)thio)benzo[1,2-b:4,5-b′]dithiophene-

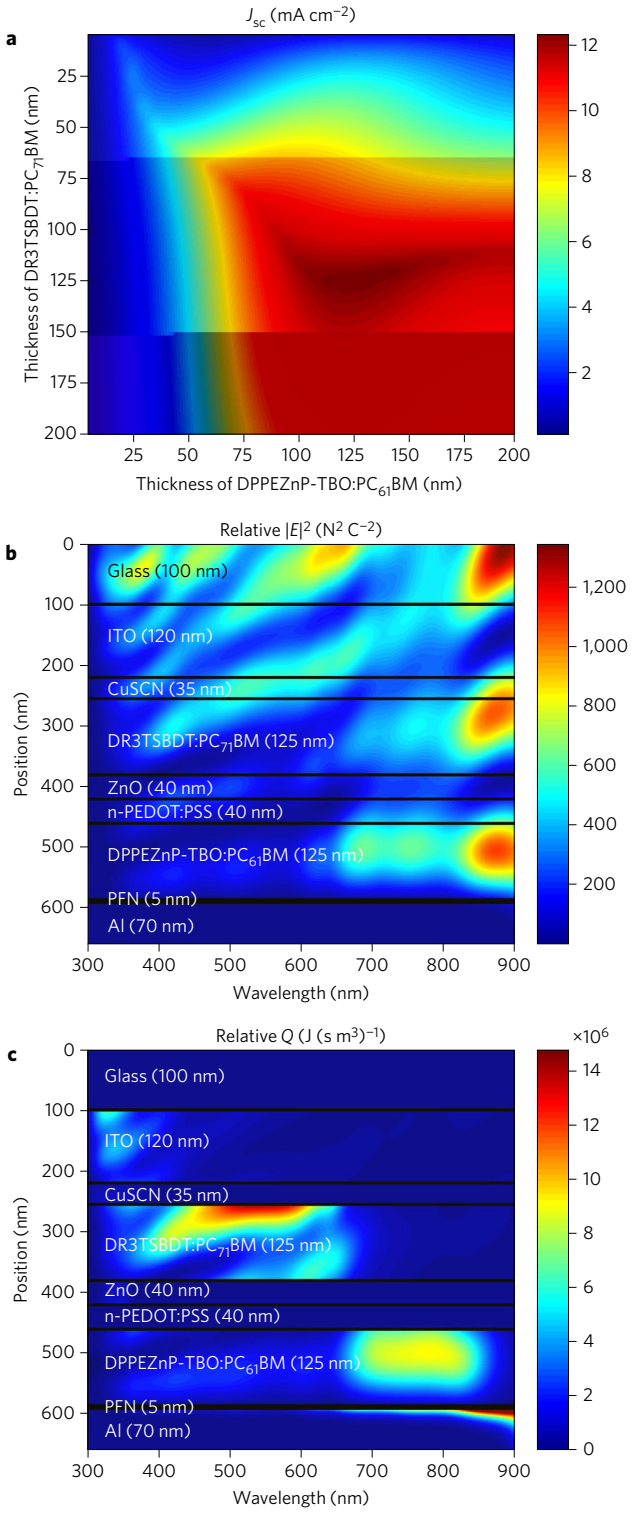

Figure 2 | Optical simulation. a, Simulated current density J_{sc} generated in the tandem device as a function of active layer thickness. **b**,**c**, Simulated distribution of the squared optical electric field (**b**) and simulated energy distribution (**c**) in the tandem device with front subcell thickness of 125 nm and rear subcell thickness of 125 nm.

2,6-diyl)bis(3,3′′-dioctyl-[2,2′:5′,2′′-terthiophene]-5′′,5-diyl))bis(methanylylidene))bis(3-ethyl-2-thioxothiazolidin-4-one) (DR3TSBDT), (5Z,5′E)-5,5′-((5′′,5′′′′′-(4,8-bis(5-(2-ethylhexyl)thiophen-2-yl)benzo[1,2-b:4,5-b′]dithiophene-2,6-diyl)bis(3,3′′-dioctyl-[2,2′:5′,2′′-terthiophene]-5′′,5-diyl))bis(methanylylidene))bis(3-ethyl-2-thioxothiazolidin-4-one) (DR3TBDTT) and (5Z,5′E)-5,5′-((5′′,5′′′′′-(4,8-bis(5-(2-hexyldecyl)thieno[3,2-b]thiophen-2-yl)benzo[1,2-b:4,5-b′]dithiophene-2,6-diyl)bis(3,3′′-dioctyl-[2,2′:5′,2′′-terthiophene]-5′′,5-diyl))bis(methanylylidene))bis(3-ethyl-2-thioxothiazolidin-4-one) (DR3TBDT-TT)) as the front subcell donors and poly[4,8-bis(5-(2-ethylhexyl)thiophen-2-yl)benzo[1,2-b:4,5-b′]dithiophene-co-3-fluorothieno[3,4-b]thiophene-2-carboxylate] (PTB7-Th) as the rear subcell donor, and PCEs of over 10% have been achieved[24]. However, a big issue for these tandem cells is the overlap of the absorption between the three small molecules in the front subcell and PTB7-Th in the rear subcell, which limits the J_{sc} of the tandem devices. Thus, a much redshifted active material with more complementary (with less overlap) absorption in the rear subcells to produce a better and more balanced J_{sc} is needed to achieve higher performance in the tandem cells with these small molecules in the front subcells. Based on such a strategy, we now report the results using two small molecules with better complementary absorption, DR3TSBDT[25] and 5,15-bis(2,5-bis(2-ethylhexyl)-3,6-dithienyl-2-yl-2,5-dihydro-pyrrolo[3,4-c]pyrrole-1,4-dione-5′-yl-ethynyl)-10,20-bis(5-(2-butyloctyl)thienyl)porphyrin zinc(II) (DPPEZnP-TBO)[26] (Fig. 1a), as the front and rear subcell donor materials in solution-processed tandem cells. The optimized device gives the highest PCE (12.50%, verified 12.70%) of all the solution-processed organic photovoltaic devices reported in the literature so far.

The absorption spectra of DR3TSBDT and DPPEZnP-TBO films are shown in Fig. 1b. The DR3TSBDT film shows an absorption window in the visible light range that extends to 700 nm. Importantly, the DPPEZnP-TBO film can absorb near-infrared photons up to 907 nm. Together, the two small molecules effectively cover the entire range of the solar spectrum up to the near-infrared region and have much better complementary absorption than the materials we used previously[24]. The performance of single-junction devices using DR3TSBDT and DPPEZnP-TBO was studied and optimized, and the current density–voltage (J–V) curves of the single-junction devices are shown in Fig. 1c, with the performance parameters detailed in Supplementary Table 1. The device based on DR3TSBDT:PC$_{71}$BM showed a PCE over 9%, with a high V_{oc} of ~0.9 V and a J_{sc} over 14 mA cm^{-2}. The device based on DPPEZnP-TBO:PC$_{61}$BM gave a higher V_{oc} (0.73 V) than other low-bandgap-material-based devices because of its small energy loss[21,26]. Note that the high J_{sc} of 18.53 mA cm^{-2} was achieved due to the broad absorption of DPPEZnP-TBO, especially in the near-infrared range. External quantum efficiency (EQE) curves of the optimized single-junction devices with DR3TSBDT:PC$_{71}$BM and DPPEZnP-TBO:PC$_{61}$BM are shown in Fig. 1d. The DR3TSBDT-based device exhibited a high EQE response in the range of 300–650 nm and the DPPEZnP-TBO-based device showed a broad EQE response from 300 to 900 nm. Importantly, the DPPEZnP-TBO-based device exhibited excellent EQE values in the range of 650–900 nm where the DR3TSBDT-based device has its most diminished EQE. These single-junction cell results indicate that if these two donor materials with better complementary absorption are used in the front and rear subcells of tandem devices, high EQEs in a wide range should be expected in the tandem cells.

Tandem devices were fabricated using all solution processing, except for the aluminium metal electrode. The tandem device architecture and corresponding energy diagram are presented in Fig. 1e,f. After a series of optimizations, copper(I) thiocyanate (CuSCN)[27] was selected as the hole transport material for the front subcell because of its high optical transparency and high hole mobility, and more importantly its better performance, and the popular poly[(9,9-bis(3′-(*N*,*N*-dimethylamino)propyl)-2,7-fluorene)-alt-2,7-(9,9-dioctylfluorene)] (PFN) was chosen as the cathode buffer layer for the DPPEZnP-TBO:PC$_{61}$BM-based rear subcell for electron extraction. A fully solution-processed interconnection layer, consisting of a ZnO nanoparticle layer deposited from n-butanol

Table 1 | Tandem device performances with different thicknesses of the subcells.

Thickness (nm)		V_{oc} (V)	J_{sc} (mA cm^{-2})	J_{sc}* (mA cm^{-2})	FF (%)	PCE (%)
Front subcell	Rear subcell					
90	125	1.623 ± 0.015	11.21 ± 0.22	9.83	63.0 ± 0.9	11.46 ± 0.28 (11.74)
125	125	1.625 ± 0.015	12.05 ± 0.24	12.31	62.7 ± 1.2	12.28 ± 0.22 (12.50, 12.16†)
150	125	1.625 ± 0.015	11.58 ± 0.25	11.45	60.4 ± 1.3	11.37 ± 0.35 (11.72)
125	90	1.624 ± 0.015	11.01 ± 0.19	10.65	63.1 ± 0.9	11.28 ± 0.28 (11.56)
125	150	1.624 ± 0.015	11.94 ± 0.26	11.84	60.8 ± 1.1	11.79 ± 0.26 (12.05)

All average values are obtained from more than 50 devices. Data in parentheses are the best PCEs. *Simulated current density from Fig. 2a; †PCE obtained with the mask.

and pH-neutral PEDOT:PSS processed from water/isopropanol, was used to connect the two subcells. Details of the materials and device fabrication are provided in the Supplementary Information and the Methods, respectively.

For serially connected tandem solar cells it is critical to obtain symmetric or balanced current densities in all the subcells, because the overall J_{sc} depends on the current in the subcells, so optical modelling of the electric field distribution within the device was first carried out to provide a guide to selecting the optimal thicknesses of the subcells. The refractive index n and extinction coefficient k of the different layers used in the tandem devices were measured by a spectroscopic ellipsometer. Figure 2a presents the simulation results for the dependence of J_{sc} on the thicknesses of the active layers. Based on the optical simulation, J_{sc} reaches an optimum value of over 12 mA cm^{-2} when the thicknesses of the optimized DR3TSBDT:$PC_{71}BM$ and DPPEZnP-TBO:$PC_{61}BM$ layers are both around 125 nm. The simulated distribution of the squared optical electric field and the simulated energy dissipation rate within the tandem device with optimized subcell thicknesses are shown in Fig. 2b and Fig. 2c, respectively. The simulation shows that the energy distribution in the front subcell is mainly localized at the wavelength range of 300–650 nm, while in the rear subcell only a small portion of energy is dissipated in the visible range and instead it is mainly localized in the near-infrared range of 650–900 nm.

With guidance from the results for the single-junction cells and the optical modelling decribed above, a series of tandem devices were fabricated, and the impact of subcell thickness on photovoltaic performance was investigated. The thickness of the front subcell active layer was tuned from 90 to 150 nm while keeping the active layer thickness of the rear subcell as 125 nm. Similarly, the thickness of the rear subcell was studied in the range from 90 to 150 nm. The detailed photovoltaic parameters are summarized in Table 1. Clearly, the first conclusion from these data is that, overall, the devices provide excellent performance, with PCEs above 11% with almost the same V_{oc} and similar FF. This indicates that the performance of our tandem cells is rather independent of active layer thickness, which is important for possible future OSC commercialization.

Note that the tandem devices all showed a V_{oc} value of ~1.62 V, which is approximately equal to the sum of the individual V_{oc} values of the subcells. The values of FF are all over 60%, which is close to that of the DPPEZnP-TBO-based single-junction device[26]. The difference in the PCEs of devices with different thicknesses mainly arises from the J_{sc}. For example, when the active layer thickness of the rear subcell was fixed at 125 nm, the V_{oc} and FF of the tandem cells showed no apparent change on increasing the thickness of the front subcell from 90 to 125 nm, but the J_{sc} increased from 11.21 to 12.05 mA cm^{-2}. However, the J_{sc} reduced to 11.58 mA cm^{-2} when the thickness of the front subcell further increased to 150 nm, indicating that the absorption of the front subcell might be too strong to leave sufficient light to generate a matched J_{sc} in the rear subcell. On the other hand, when the active layer thickness of the front subcell was fixed at 125 nm, the tandem device with a rear subcell thickness of 90 nm showed a relatively lower J_{sc} of 11.01 mA cm^{-2} due to the limited absorption of the rear subcell. When the rear subcell thickness increased from 125 to 150 nm, the tandem devices retained a high J_{sc} of ~12 mA cm^{-2}, but the FF decreased from 62.7 to 60.8%, leading to a decreased PCE of 12.05%. These experimental results match the optical simulation very well (Fig. 2). As shown in Fig. 3a, the tandem device with an optimized subcell thickness of 125 nm for the active layer of both front and rear subcells exhibited high PCEs of 12.50% without a mask and 12.16% with a mask. The above results were verified by the National Institute of Metrology (NIM), with measured PCE values of 12.70 and 12.59% without and with a mask, respectively (Supplementary Figs 3 and 4). Importantly, as shown in Table 1, the optimized tandem device performance is reproduced very well with a small variation in the key photovoltaic parameters (V_{oc}, J_{sc}, FF and PCE), with the average values based on more than 50 devices being very similar to the best results obtained. Furthermore, a series of tandem devices with large areas were fabricated and tested (Supplementary Table 3) and a PCE of nearly 11% was achieved for devices with a centimetre-square area.

To further comprehend the reasons for the excellent performance, the EQEs of the front and rear subcells in the tandem

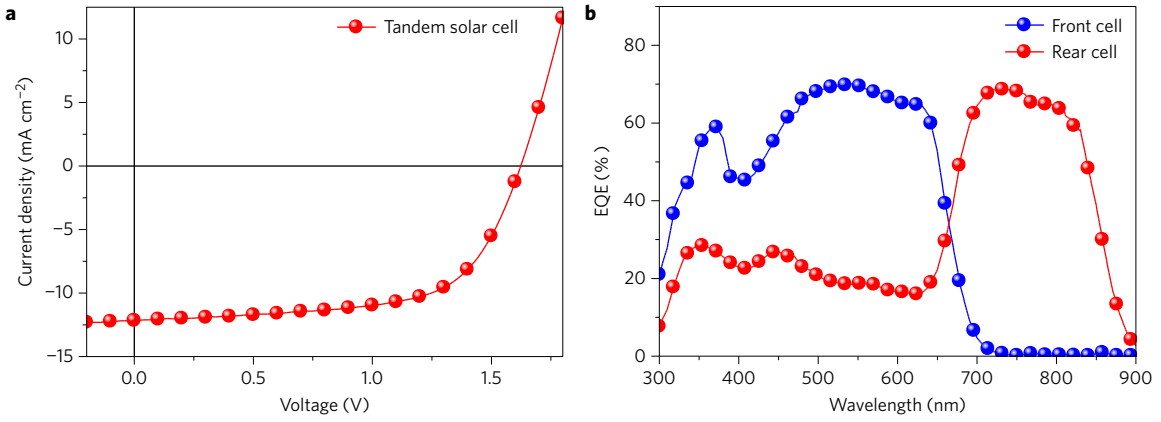

Figure 3 | Photovoltaic performance of the tandem solar cell. a,**b**, *J*–*V* curve (**a**) and EQE curve (**b**) of the optimized tandem solar cell.

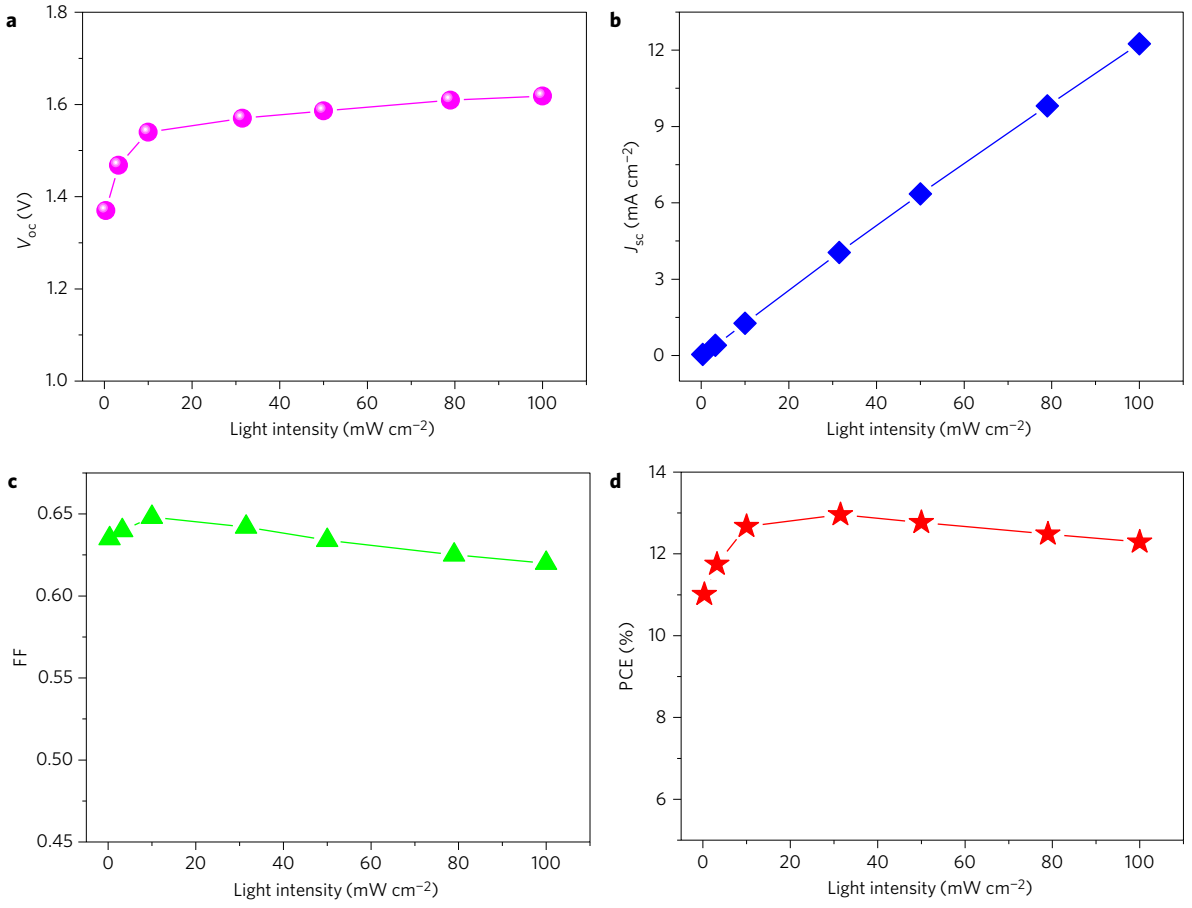

Figure 4 | Tandem device performance parameters under different light intensities. a–d, Variation of V_{oc} (**a**), J_{sc} (**b**), FF (**c**) and PCE (**d**) of the tandem device under different light intensities from 0.32 to 100 mW cm^{-2}.

device were measured using light bias obtained using 700 nm high-pass and 600 nm low-pass optical filters, respectively[28]. As shown in Fig. 3b, the front subcell absorbs most of the high-energy photons within the range of 300–650 nm, and its maximum response reaches ~70% at 540 nm. The rear subcell absorbs most of the low-energy photons (from ~650 to 900 nm), with a strong EQE response over 60% in the range of 690–820 nm. The rear subcell still shows 15–25% EQE in the range of 400–650 nm due to the overlap of the absorption spectra of DR3TSBDT and DPPEZnP-TBO in this range. The J_{sc} values obtained by integration of the EQE curves are 11.53 mA cm^{-2} for the front subcell and 11.95 mA cm^{-2} for the rear subcell, suggesting highly balanced current generation in each subcell. The EQE-integrated current densities of the subcells are consistent with the J_{sc} of the tandem solar cell measured under AM 1.5G illumination. Importantly, these results are consistent with the EQE results (Fig. 1d) for the single-junction cells and the optical simulation (Fig. 2), and further indicate that our tandem cell design strategy using donor materials with better complementary absorption and balanced currents in the front and rear subcells is effective. Note that it is vital to characterize all high-performance OSC materials and their devices and have reliable and repeatable results following creditable protocols/standards. Thus, for the measurements and characterization in this work for the more complicated tandem devices, recent proposals[29] have been used as a guide (for details see the Methods).

Given that solar irradiation varies throughout the day, the performance of the tandem device under different illumination intensities was also evaluated. As shown in Fig. 4, the light intensity dependence of the J_{sc}, V_{oc} and FF of the tandem cells shows a behaviour similar to that reported for high-performance single-junction devices[30]. The PCE of the tandem device is maintained at over 11% when the light intensity varies from 100 to 0.32 mW cm^{-2}, and reaches 12.96% at a light intensity of 31.5 mW cm^{-2}. The higher performance achieved with lower light intensities indicates that the tandem device can work well to efficiently harvest sunlight under varying light intensities.

In conclusion, we have demonstrated an all-small-molecule tandem device with a PCE of 12.50% (verified 12.70%) under 1 sun condition and ~13% under 0.3 sun condition. Importantly, the high performance of the solution-processed tandem solar cells barely changes with different thicknesses of both the front and rear subcells and under different light intensities. Note that both the FF and J_{sc} in the tandem cells are still lower than the best measured in corresponding single-junction cells, particularly the FF. This indicates that further optimization, including better interconnection layers and better but more balanced donor materials with complementary absorption, would enhance the tandem device performance further and thus warrants much more investigation. Combined with other advantages of small-molecule-based devices, these results demonstrate that small-molecule-based tandem cells might be a very competitive alternative in the pursuit of possible future OSC commercialization.

Methods

Methods and any associated references are available in the online version of the paper.

Received 27 June 2016; accepted 1 November 2016; published online 5 December 2016; corrected online 19 December 2016

References

1. You, J., Dou, L., Hong, Z., Li, G. & Yang, Y. Recent trends in polymer tandem solar cells research. *Prog. Polym. Sci.* **38,** 1909–1928 (2013).
2. Service, R. F. Outlook brightens for plastic solar cells. *Science* **332,** 293 (2011).
3. He, Z. *et al.* Single-junction polymer solar cells with high efficiency and photovoltage. *Nat. Photon.* **9,** 174–179 (2015).
4. Zhao, J. *et al.* Efficient organic solar cells processed from hydrocarbon solvents. *Nat. Energy* **1,** 15027 (2016).
5. Kan, B. *et al.* A series of simple oligomer-like small molecules based on oligothiophenes for solution-processed solar cells with high efficiency. *J. Am. Chem. Soc.* **137,** 3886–3893 (2015).
6. Zhang, S. *et al.* Realizing over 10% efficiency in polymer solar cell by device optimization. *Sci. China Chem.* **58,** 248–256 (2015).
7. You, J. *et al.* A polymer tandem solar cell with 10.6% power conversion efficiency. *Nat. Commun.* **4,** 1446 (2013).
8. Zheng, Z. *et al.* Highly efficient tandem polymer solar cells with a photovoltaic response in the visible light range. *Adv. Mater.* **27,** 1189–1194 (2015).
9. Yusoff, A. B. *et al.* A high efficiency solution processed polymer inverted triple-junction solar cell exhibiting a power conversion efficiency of 11.83%. *Energy Environ. Sci.* **8,** 303–316 (2015).
10. Chou, C.-H., Kwan, W. L., Hong, Z., Chen, L.-M. & Yang, Y. A metal-oxide interconnection layer for polymer tandem solar cells with an inverted architecture. *Adv. Mater.* **23,** 1282–1286 (2011).
11. Zuo, L. *et al.* Design of a versatile interconnecting layer for highly efficient series-connected polymer tandem solar cells. *Energy Environ. Sci.* **8,** 1712–1718 (2015).
12. Kouijzer, S. *et al.* Efficient inverted tandem polymer solar cells with a solution-processed recombination layer. *Adv. Energy Mater.* **2,** 945–949 (2012).
13. Zhou, H. Q. *et al.* Polymer homo-tandem solar cells with best efficiency of 11.3%. *Adv. Mater.* **27,** 1767–1773 (2015).
14. Li, N. *et al.* Design of the solution-processed intermediate layer by engineering for inverted organic multi junction solar cells. *Adv. Energy Mater.* **3,** 301–307 (2013).
15. Gilot, J., Wienk, M. M. & Janssen, R. A. J. Optimizing polymer tandem solar cells. *Adv. Mater.* **22,** E67–E71 (2010).
16. Gevaerts, V. S., Furlan, A., Wienk, M. M., Turbiez, M. & Janssen, R. A. J. Solution processed polymer tandem solar cell using efficient small and wide bandgap polymer:fullerene blends. *Adv. Mater.* **24,** 2130–2134 (2012).
17. Dou, L. *et al.* Tandem polymer solar cells featuring a spectrally matched low-bandgap polymer. *Nat. Photon.* **6,** 180–185 (2012).
18. Zheng, Z. *et al.* Over 11% efficiency in tandem polymer solar cells featured by a low-band-gap polymer with fine-tuned properties. *Adv. Mater.* **28,** 5133–5138 (2016).
19. Mishra, A. & Bäuerle, P. Small molecule organic semiconductors on the move: promises for future solar energy technology. *Angew. Chem. Int. Ed.* **51,** 2020–2067 (2012).
20. Lin, Y. & Zhan, X. Oligomer molecules for efficient organic photovoltaics. *Acc. Chem. Res.* **49,** 175–183 (2016).
21. Gao, K. *et al.* Deep absorbing porphyrin small molecule for high-performance organic solar cells with very low energy losses. *J. Am. Chem. Soc.* **137,** 7282–7285 (2015).
22. Liu, Y. *et al.* Solution-processed small-molecule solar cells: breaking the 10% power conversion efficiency. *Sci. Rep.* **3,** 3356 (2013).
23. Riede, M. *et al.* Efficient organic tandem solar cells based on small molecules. *Adv. Funct. Mater.* **21,** 3019–3028 (2011).
24. Zhang, Q. *et al.* Evaluation of small molecules as front cell donor materials for high-efficiency tandem solar cells. *Adv. Mater.* **28,** 7008–7012 (2016).
25. Kan, B. *et al.* Solution-processed organic solar cells based on dialkylthiol-substituted benzodithiophene unit with efficiency near 10%. *J. Am. Chem. Soc.* **136,** 15529–15532 (2014).
26. Gao, K. *et al.* Multi-length-scale morphologies driven by mixed additives in porphyrin-based organic photovoltaics. *Adv. Mater.* **28,** 4727–4733 (2016).
27. Pattanasattayavong, P., Mottram, A. D., Yan, F. & Anthopoulos, T. D. Study of the hole transport processes in solution-processed layers of the wide bandgap semiconductor copper(I) thiocyanate (CuSCN). *Adv. Funct. Mater.* **25,** 6802–6813 (2015).
28. Gilot, J., Wienk, M. M. & Janssen, R. A. J. Measuring the external quantum efficiency of two-terminal polymer tandem solar cells. *Adv. Funct. Mater.* **20,** 3904–3911 (2010).
29. Timmreck, R. *et al.* Characterization of tandem organic solar cells. *Nat. Photon.* **9,** 478–479 (2015).
30. Zhang, Q. *et al.* Small-molecule solar cells with efficiency over 9%. *Nat. Photon.* **9,** 35–41 (2015).

Acknowledgements

The authors acknowledge financial support from MoST (2014CB643502, 2016YFA0200200), NSFC (51373078, 51422304, 91433101, 51323003, 51473053) and the International Science and Technology Cooperation Program of China (2013DFG52740).

Author contributions

M.L. fabricated and characterized the devices with help from Q.Z. K.G. synthesized the donor material DPPEZnP-TBO. B.K. synthesized the donor material DR3TSBDT. X.Y. and H.F. prepared the ZnO electron transport material. J.P. and Z.L. performed the experiments on the measurement of *n* and *k*. H.Y. performed the optical simulations. Y.Ch. and X.W. supervised and coordinated the study. All authors discussed the results and commented on the manuscript.

Additional information

Supplementary information is available in the online version of the paper. Reprints and permissions information is available online at www.nature.com/reprints. Correspondence and requests for materials should be addressed to X.W., X.P. and Y.Ch.

Competing financial interests

The authors declare no competing financial interests.

Methods

Measurements and instruments. Current density–voltage (J–V) curves of photovoltaic devices were obtained by a Keithley 2400 source-measure unit. Photocurrent was measured under illumination with simulated 100 mW cm^{-2} AM 1.5G irradiation using a SAN-EI XES-70S1 solar simulator. EQEs were measured using a Beijing Sevenstar EQE measurement system. The thickness of the active layers in the photovoltaic devices was measured on a Veeco Dektak 150 profilometer. The optical model was performed based on a transfer matrix formalism model. The refractive index n and extinction coefficient k spectra for each layer in the devices were measured using a J.A. Woolam Co. V-VASE ellipsometer (VB-400 Control Module).

Fabrication of single-junction devices. The DR3TSBDT:$PC_{71}BM$ single cell was fabricated with device architectures of ITO/CuSCN or PEDOT:PSS/DR3TSBDT:$PC_{71}BM$/PFN/Al. A thin layer (35 nm) of CuSCN processed from dimethyl sulfide solution was spin-coated on top of pre-cleaned ITO substrates and annealed in air at 120 °C for 10 min. The hole transport layer (40 nm) of PEDOT:PSS (Clevios PVP AI 4083) was spin-coated at 4,000 r.p.m. and annealed in air at 150 °C for 10 min. The active layer was spin-coated from blend chloroform solutions with a weight ratio of DR3TSBDT and $PC_{71}BM$ of 1:0.8. Thermal annealing was carried out on a digitally controlled hotplate at 90 °C, and the substrates were then placed in a glass Petri dish containing 150 µl chloroform for solvent vapour annealing for 60 s. For the DPPEZnP-TBO-based device, the device architecture was ITO/PEDOT:PSS/DPPEZnP-TBO:$PC_{61}BM$/PFN/Al. The active layer was spin-coated from chlorobenzene solution (0.4% pyridine and 0.4% 1,8-diiodooctane (DIO) by volume) with a weight ratio of DPPEZnP-TBO and $PC_{61}BM$ of 1:1. A thin layer (~5 nm) of PFN was spin-coated from methanol solution (0.2% acetic acid by volume) on the top of active layers. Finally, a 70 nm Al layer was deposited under high vacuum (<1.5×10^{-4} Pa).

Fabrication of tandem devices. The tandem devices were fabricated with an architecture of glass/ITO/CuSCN/DR3TSBDT:$PC_{71}BM$/ZnO/PH neutral PEDOT:DPPEZnP-TBO:$PC_{61}BM$/PFN/Al. The DR3TSBDT:$PC_{71}BM$ active layers were fabricated with different thicknesses via the same process as the single cells. Subsequently, the ZnO nanoparticle layer (40 nm) was spin-coated on top of the active layer of the front subcell, and then n-PEDOT:PSS (~40 nm) was spin-coated. The DPPEZnP-TBO:$PC_{61}BM$ active layers were fabricated with different thicknesses via the same process as the single cells. A thin layer (~5 nm) of PFN was spin-coated on top of the DPPEZnP-TBO:$PC_{61}BM$ active layer. Finally, the devices were completed after deposition of 70 nm Al as the cathode. The effective areas of the cells were ~4 mm^2, as defined by shallow masks.

Tandem device characterization. The current density–voltage (J–V) curves of photovoltaic devices were obtained using a Keithley 2400 source-measure unit. Photocurrent was measured under illumination with simulated 100 mW cm^{-2} AM 1.5G irradiation using a SAN-EI XES-70S1 AAA class solar simulator, calibrated with a reference Si solar cell. The reference cell was a KG-5 filter silicon diode, which was calibrated and certified by the National Center of Supervision & Inspection on Solar Photovoltaic Products Quality of China (CPVT). The spectral irradiance of the simulator light source and the AM 1.5G spectrum are presented in Supplementary Fig. 1. The values of mismatch factor M for both subcells under the solar simulator were calculated according to ref. 31, and the values were ~1 (0.98 for the front cell and 1.03 for the rear cell). J–V measurements were carried out with and without a mask (~3.24 mm^2) on the optimized tandem devices, and the detailed photovoltaic parameters are summarized in Supplementary Table 2. The PCE of the tandem cell with the mask was 3% lower than that without the mask.

For J–V measurements under different light intensities, neutral density filters were used to tune the light intensity and a standard Si solar cell was used to calibrate the light intensity.

The EQEs of both subcells were measured using chopped monochromatic light in conjunction with the lock-in technique applying the determined bias light conditions. Light bias obtained by 600 nm low-pass and 700 nm high-pass optical filters was selected to excite (saturate) the front and rear cells to measure the rear and front cells, respectively. The intensity of the bias light was adjusted using a variable-neutral density filter. The bias intensity was ~4 mW cm^{-2}. A bias voltage was not applied in the EQE measurements of the front and rear subcells in the tandem device because, in our cases, the shunt resistances for the subcells were as high as ~10^5 Ω cm^{-2} (calculated from J–V measurements under dark conditions). It is not necessary to apply a bias voltage to avoid overestimation[17]. Thus, EQE measurements using bias light only were conducted, and the J_{sc} from the EQE could be obtained. We also measured the EQE without bias light (Supplementary Fig. 2), and the spectral response was indeed much lower than that with bias light.

The optimized tandem device performances without and with mask (Supplementary Figs 3 and 4) were verified by the National Institute of Metrology (NIM) of China and the results are consistent with those obtained in our laboratory.

References

31. Shrotriya, V. *et al.* Accurate measurement and characterization of organic solar cells. *Adv. Funct. Mater.* **16,** 2016–2023 (2006).

Erratum: Solution-processed organic tandem solar cells with power conversion efficiencies >12%

Miaomiao Li, Ke Gao, Xiangjian Wan, Qian Zhang, Bin Kan, Ruoxi Xia, Feng Liu, Xuan Yang, Huanran Feng, Wang Ni, Yunchuang Wang, Jiajun Peng, Hongtao Zhang, Ziqi Liang, Hin-Lap Yip, Xiaobin Peng, Yong Cao and Yongsheng Chen

Nature Photonics http://dx.doi.org/10.1038/nphoton.2016.240 (2016); published online 5 December 2016;
corrected online 19 December 2016.

In the version of this Letter originally published online, in Fig. 1c, the bottom two values on the *y* axis were incorrect. This has now been corrected in all versions of the Letter.